CONFERENCE PRE-PRINT

H-MODE OPERATION SCENARIOS IN JT-60SA INITIAL RESEACH PHASE PREDICTED BY INTEGRATED CORE-PEDESTAL-SOL/DIVERTOR SIMULATION

N. Aiba, S. Yamoto, N. Hayashi, D. Umezaki, T. Nakano, T. Wakatsuki National Institutes for Quantum Science and Technology Naka/Ibaraki, Japan Email: aiba.nobuyuki@qst.go.jp

S. Saarelma United Kingdom Atomic Energy Authority Abingdon, United Kingdom

M. Honda Graduate School of Engineering, Kyoto University Kyoto/Kyoto, Japan

L. Frassinetti, A. Lafay-Labrosse Division of Fusion Plasma Physics, KTH Royal Institute of Technology Stockholm, Sweden

K. Hoshino Faculty of Science and Technology, Keio University Yokohama/Kanagawa, Japan

Abstract

Accurate prediction of stationary plasma scenarios that meet both performance and engineering constraints is crucial for future fusion reactors. We present an extension of GOTRESS+, an integrated simulation framework for JT-60SA, which couples core transport, pedestal structure, and SOL/divertor physics using models such as EPED1, the Saarelma–Connor model, IMPACT, and SONIC. This enables self-consistent evaluation of plasma profiles and boundary conditions across all regions. We apply GOTRESS+ to predict H-mode scenarios in JT-60SA's initial research phase, focusing on hybrid and baseline cases. The hybrid scenario achieves high performance without extrinsic impurity injection, maintaining divertor heat loads below limits via optimized deuterium fueling. The baseline scenario, with higher heating power and plasma current, requires increased fueling or neon seeding to meet exhaust constraints. In both scenarios, predicted plasma parameters exceed target thresholds for normalized beta and confinement, confirming JT-60SA's feasibility under ITER/DEMO-relevant conditions. These results highlight the value of integrated modeling and establish JT-60SA as a testbed for predictive simulations. GOTRESS+ serves as a robust tool for experimental planning and future reactor design.

1. INTRODUCTION

Power exhaust control remains a fundamental yet critical challenge in the development of large-scale fusion reactors. As fusion power output increases—particularly in devices aiming for fusion power levels of $P_{fus} \ge 1 GW$ —the associated heat flux to the scrape-off layer (SOL) and divertor regions (q_{\parallel}) becomes substantial, necessitating robust mitigation strategies. Accurate prediction and control of plasma density across different regions of the reactor are essential for achieving optimal performance and sustaining fusion reactions.

Core plasma density prediction has advanced through transport models like TGLF [1] and QuaLiKiz [2], enabling reliable simulations under various scenarios. For the SOL and divertor, codes such as SOLPS-ITER [3] and SONIC [4] have been used to evaluate density profiles that meet engineering and physical constraints. However, pedestal density prediction—serving as the boundary condition for core transport models—remains unresolved, limiting the accuracy of integrated modeling and overall plasma predictability.

To mitigate intense SOL/divertor heat flux, injecting mid-to-high-Z impurity ions has proven effective [5,6], enhancing radiative cooling and reducing q_{\parallel} below engineering limits. On the other hand, these impurities can

degrade core performance by diluting fuel and increasing radiation losses. Thus, precise control of impurity transport and concentration is vital—not only to protect plasma-facing components but also to maintain core quality and fusion gain, even in ITER.

JT-60SA is uniquely suited for validating physics-based integrated code suites. Designed to explore long pulse steady-state, high-performance plasmas, it supports the development of non-inductive, high-beta scenarios under ITER/DEMO-relevant conditions [7]. The JT-60SA program aims to establish high performance scenarios that: (i) meet divertor heat load constraints under ITER relevant conditions, (ii) achieve DEMO-relevant metrics such as confinement enhancement factor $H_{98y2} > 1.3$ and bootstrap current fraction $f_{BS} > 0.6$, and (iii) operate above the no-wall ideal MHD beta limit. These capabilities make JT-60SA a key platform for demonstrating ITER/DEMO feasibility through physics understanding and control strategy development.

To date, 1.5D transport simulations have been performed for JT-60SA's flat-top phase using integrated modeling frameworks like JINTRAC [8], TOPICS [9], and others; recent results can be found in [10,11]. These simulations generally align with expected scenario projections, with discrepancies in key 0-D parameters within 40%, assuming similar H-mode pedestal characteristics. This highlights the importance of accurately predicting pedestal conditions compatible with SOL/divertor plasmas—a key issue to be validated in upcoming experiments.

To enhance predictive capability for stationary scenarios, we extended the GOTRESS+ simulation suite [12] by integrating the Saarelma pedestal density model [13] and the SONIC SOL/divertor code. This enhanced framework couples models across core, pedestal, and SOL/divertor regions, enabling self-consistent evaluation of plasma profiles and boundary conditions. It has been applied to predict stationary plasma conditions for JT-60SA's initial research phase.

2. A STATIONARY TOKAMAK PREDICTOR BASED ON GOTRESS+

The GOTRESS+ code suite is designed to evaluate stationary-state performance in tokamak plasmas by integrating multiple simulation tools. At its core is GOTRESS, a transport code that solves steady-state thermal transport equations using global optimization techniques, such as genetic algorithms, to generate self-consistent plasma profiles [14]. To enhance its predictive capability, GOTRESS+ incorporates ACCOME, which calculates magnetic equilibrium consistent with current density profiles driven by auxiliary heating systems [15]. ACCOME includes a bounce-averaged Fokker–Planck solver and an electron cyclotron heating (ECH) module. The suite also integrates OFMC, which evaluates heating, fueling, and torque contributions from neutral beam injection (NBI) [16]. EPED1 is used to estimate pedestal height and width and is widely recognized as a successful semi-empirical model for pedestal prediction [17]. Together, these components enable self-consistent plasma profile calculations from the last closed flux surface to the magnetic axis, supporting comprehensive scenario modeling that accounts for transport, equilibrium, heating, and pedestal physics—making GOTRESS+ a powerful tool for optimizing stationary plasma conditions in advanced tokamak experiments like JT-60SA.

To support predictive modeling of scenarios that meet both performance targets and power exhaust constraints, additional models are needed to handle particle and impurity transport across the core, pedestal, and SOL/divertor regions, as well as thermal transport in the SOL/divertor.

To meet these requirements, GOTRESS+ has been enhanced with three key components: the IMPACT code for impurity transport [18], the Saarelma–Connor model for pedestal density prediction [13], and the SONIC code for integrated SOL/divertor simulations [4]. IMPACT calculates radial impurity transport, accounting for diffusive, convective, ionization, and recombination processes within the last closed flux surface (LCFS). It solves the one-dimensional radial continuity equation for each ionization stage, incorporating neoclassical diffusivities and pinch velocities from NCLASS [19], with optional anomalous transport.

The Saarelma–Connor model, based on the neutral ionization framework by Groebner and Mahdavi [20], predicts the radial electron density profile in the H-mode pedestal by balancing diffusion—via a spatially varying coefficient D_{ped} —against ionization. D_{ped} comprises three components: (1) D_{ETG} , driven by electron temperature gradient (ETG) modes; (2) $D_{e,NC}$, a neoclassical term; and (3) D_{KBM} , driven by kinetic ballooning modes (KBM), scaling with the normalized pressure gradient α exceeding the KBM threshold. Ionization sources include low-energy Franck–Condon neutrals and higher-energy charge exchange neutrals, with densities n_{FC} and n_{CX} , respectively. Neutral densities are modeled by balancing inward convection with ionization and charge exchange processes, enabling physics-based pedestal density estimation for core transport simulations.

SONIC is a two-dimensional SOL/divertor simulation tool [4, 21], featuring a Monte Carlo (MC) particle approach in its impurity code IMPMC, which allows flexible modeling of wall interactions and kinetic effects. IMPMC provides boundary conditions for IMPACT by supplying flux-surface-averaged impurity densities at the LCFS for each charge state i, denoted as $n_{imp,i}$.

GOTRESS+ supplies SONIC with the power crossing the separatrix, $P_{sep} = P_H - P_{rad,core}$, and the number of deuterium particles injected via NBI. SONIC then determines separatrix conditions—electron density n_(e,sep), electron temperature $T_{e,sep}$, and ion temperature $T_{i,sep}$ —which are passed to EPED1 and the Saarelma-Connor model to compute pedestal profiles. GOTRESS uses these pedestal parameters ($n_{e,ped}$, $T_{e,ped}$, $T_{i,ped}$) and impurity profiles from IMPACT to perform core transport simulations. The resulting core/pedestal predictions update P sep, prompting SONIC and other models to rerun iteratively until convergence is achieved.

This enhancement enables GOTRESS+ to self-consistently evaluate the interplay between core performance and edge power exhaust, supporting the development of stationary plasma scenarios that meet both physical and engineering constraints in JT-60SA and future reactors like ITER and DEMO.

3. PREDICTION OF OPERATION SCENARIOS IN JT-60SA INITIAL RESEARCH PHASE

3.1. JT-60SA operation scenarios in initial research phase and simulation conditions

For the initial research phase of JT-60SA, known as Operational Phase 2 (OP2), several target operation plans have been formulated to support ITER/DEMO contributions and address key scientific goals. These plans explore various confinement and current drive regimes under realistic engineering constraints. Table 1 outlines three representative scenarios: baseline, hybrid, and advanced internal transport barrier (ITB). All require H-mode operation to meet performance targets, making accurate pedestal profile prediction essential. Scenario development must also consider engineering limits—specifically, total heating and current drive power capped at 26.5 MW, and a parallel heat load limit of $q_{\parallel} \leq 10~MWm^{-2}$ on the first lower carbon divertor for up to 5 seconds.

This study focuses on predicting stationary plasma conditions for the baseline and hybrid scenarios, ensuring they meet both performance and power exhaust requirements. The baseline scenario assumes a plasma current of 4.6MA and a toroidal field of 2.25T, with total heating power $P_H = 26.5MW$ (10MW NNB, 13.5MW PNB, 3MW ECH), and shaping parameters $\kappa = 1.9, \delta = 0.55$. The hybrid scenario operates at 2.7MA and 1.7T, with $P_H = 16.5MW$ (10MW NNB, 3.5MW PNB, 3MW ECH), and $\kappa = 1.8, \delta = 0.51$.

The required power for L-H transition in deuterium plasmas is evaluated as the twice of the threshold power for L-H transition $P_{LH,08}$ defined as

$$P_{LH,08} = 0.049 n_{e20}^{0.72} B_t^{0.8} S^{0.96},$$

where n_{e20} is the line average electron density in $10^{20} \, \mathrm{m}^{-3}$, B_t is the toroidal magnetic field in T, and S is the plasma surface area in m^2 [22]. As mentioned above, the plasma shape, P_H and B_t are already assumed, this threshold power determines the maximum n_{e20} and the Greenwald density fraction of line average electron density f_{GW} as ~ 0.89 ($f_{GW} \sim 0.8$) for baseline and ~ 0.62 ($f_{GW} \sim 0.95$), respectively.

The simulation setups are as follows. As the transport model used for thermal transport in core region with GOTRESS, we applied the modified version of the mixed Bohm-gyroBohm model [23], which was validated successfully against several JET/JT-60U discharges [24, 25]. It is important to note these validations discharges were conducted under carbon wall conditions and without the use of extrinsic impurity injection. For the pedestal prediction, we used EPED1 model for pressure and the Saarelma-Connor model for density. In EPED1 model, the coefficient required to determine the pedestal width with $\Delta_{ped} = C_{ped} \sqrt{\beta_{p,ped}}$ is specified later, where $\Delta_{\Psi ped}$ is the pedestal width in the poloidal magnetic flux normalized as 0 (1) on axis (LCFS), ψ_N , $\beta_{p,ped}$ is the poloidal

	Ip/Bt (q95)	β_N/β_P	H98(y,2)	$f_{ m GW}$
OP2 baseline	4.6 MA/2.28 T (q ₉₅ ~ 3)	~2/<1	~ 1	0.4-0.6
OP2 hybrid	2.7 MA/1.70 T (q ₉₅ ~ 4)	~ 2-3/~1	> 1.1	> 0.4
OP2 ITB	1.7-2.0 MA/1.70 T $(q_{95} > 6)$	> 3.5/>>1	> 1.2	> 0.5

TABLE 1. Summary of plasma parameters of operation scenarios for JT-60SA OP2

beta at the pedestal top. The ratio between ion and electron temperature is assumed to be $(T_{i,ped} - T_{i,sep})/(T_{e,ped} - T_{e,sep}) = 1.0$, where the subscript ped (sep) indicates the value at pedestal top (separatrix), respectively. In Saarelma-Connor model, a neoclassical model by Redl was used for evaluating $D_{e,NC}$ [26], D_{KBM} is assumed as 0.1, and D_{ETG} is determined as

$$D_{ETG} = 0.5 \frac{P_{tot,e}}{Sn_e \nabla T},$$

where $P_{tot,e}$ is the total heat power to electrons.

In the impurity simulation using IMPACT, the impurity diffusivities and convective velocities are modeled as the sum of neoclassical and anomalous (turbulent) components as $D_{imp} = D_{imp,NC} + D_{imp,an}$, $v_{imp} = v_{imp,nc} + v_{imp,an}$. The neoclassical components are evaluated using NCLASS as described previously. The anomalous components are specified as follows: inside the pedestal top, diffusivity is set equal to electron diffusivity calculated using a mixed Bohm-gyroBohm model, while in the pedestal region, anomalous transport is assumed to be negligible and thus set to zero. Ionization and recombination reaction rates, $\langle \sigma v \rangle_{ion}$ and $\langle \sigma v \rangle_{rec}$ and their radiations are evaluated using ADPAK [27].

For the SOL/divertor simulation with SONIC, the radial diffusivities of ions is assumed to be $D_{i,SOL}=0.3 \mathrm{m}^2 \mathrm{s}^{-1}$ and the thermal conductivities for both ions and electrons are set to $\chi_{i,SOL}=\chi_{e,SOL}=1.0 \mathrm{m}^2 \mathrm{s}^{-1}$; these are typical values used to reproduce JT-60U experiments [28] and are used in JT-60SA [18] and ITER simulations [29]. In the current version, SONIC does not include drift effects for bulk ions, although the effects for impurities are taken into account. The gas pumping speed is assumed to be $50 m^3/s$, corresponding to half of the full capability of the JT-60SA complete pumping system, and the D2 fueling rate Γ_{D2} is varied up to $13.6 \times 10^{21} \mathrm{s}^{-1}$ in this study, to identify the minimum rate required to sufficiently reduce q_{\parallel} .

3.2. Hybrid scenario prediction

First, we predict the JT-60SA hybrid scenario, because, as suggested by the Eich scaling [30], the plasma having lower I_p is favourable to satisfy q_{\parallel} below the engineering limit (=10MW m^{-2}) because of wider SOL width λ_q . In this study, no extrinsic impurity was injected, hence the deuterium and intrinsic "carbon" impurity are the ion species considered.

First, we examined the plasma condition in SOL/divertor region using SONIC. Figure 1 (a) shows the dependence of q_{\parallel} on Γ_{D2} . As indicated by the blue curve, q_{\parallel} can be reduced below $10MW~m^{-2}$ by injecting D2 at rates $\Gamma_{D2} \geq 5.5 \times 10^{20} s^{-1}$. Figure 1 (b) presents a two-dimensional plot of radiation power density for the case with $\Gamma_{D2} = 5.5 \times 10^{21} s^{-1}$. As shown, large radiation is localized near the divertor plate on the low field side (LFS) of the SOL. This localized radiation leads to an attached condition, indicating that detachment is not achieved under these fueling conditions. Under these conditions, the bulk plasma parameters at the LCFS are $n_{e,sep} = 2.35 \times 10^{19} m^{-3}$, $T_{e,sep} = 0.17 \text{keV}$, $T_{i,sep} = 0.21 \text{keV}$. The $n_{e,sep}$ value is used as the input parameter for Saarelma-Connor model predicting $n_{e,ped}$, and as shown in Fig. 2, the quantity is determined as $n_{e,ped} = 5.05 \times 10^{19} m^{-3}$. This density at the pedestal top is used in the prediction of pedestal of pressure (and temperature) using EPED1.

In addition, the SOL/divertor simulation determined the flux averaged density of impurity species at the LCFS as follows: $n_{C4+} = 5.94 \times 10^{16} m^{-3}$, $n_{C5+} = 1.15 \times 10^{17} m^{-3}$ and $n_{C6+} = 7.41 \times 10^{16} m^{-3}$

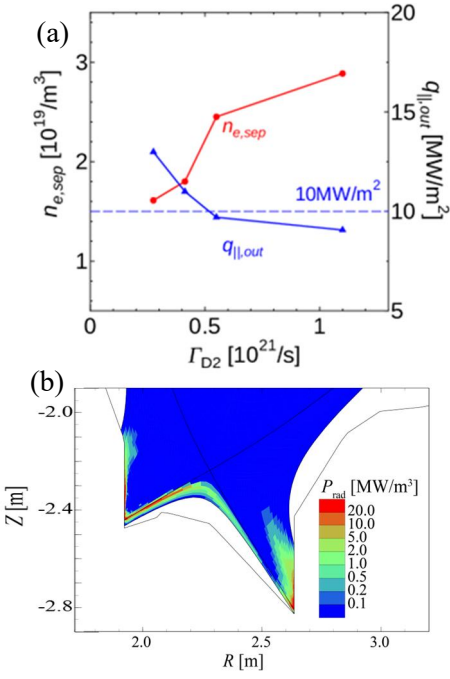


Figure 1: (a) Dependence of q_{\parallel} and $n_{e,sep}$ on Γ_{D2} . (b) 2D plot of radiator power density in SOL/divertor region.

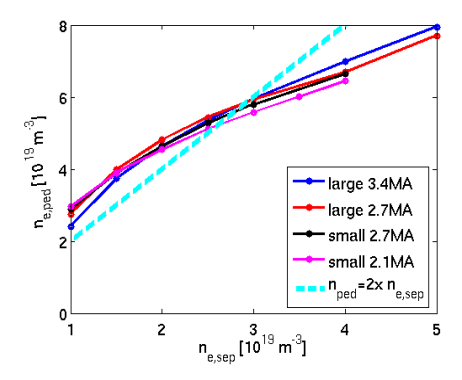


Figure 2: (a) Dependence of $n_{e,ped}$ on $n_{e,sep}$.

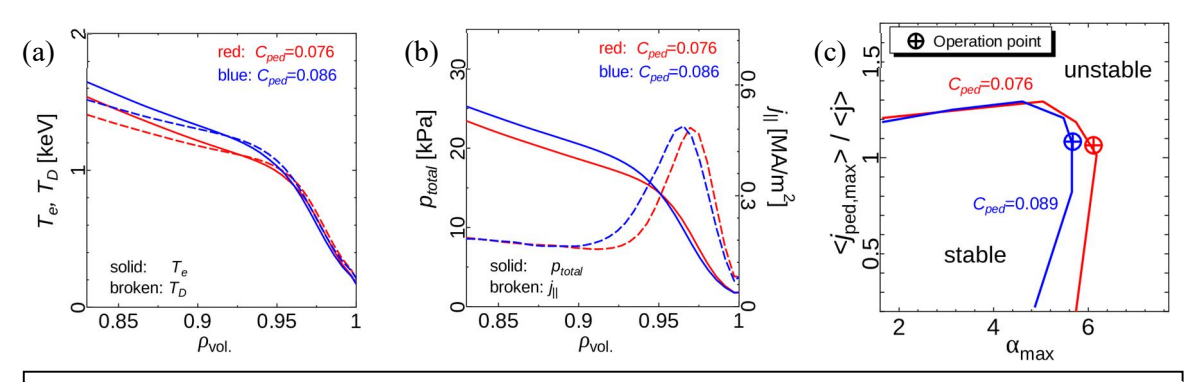


Figure 3: (a), (b) Plasma profiles at edge pedestal of JT-60SA OP2 hybrid scenario plasma; (a) T_e and T_i , (b) p and j_{\parallel} . (c) Pedestal MHD stability diagram in the (j_{ped}, α) plane.

 $10^{17}m^{-3}$. Note that the density of C_0 , C_{1+} , C_{2+} , C_{3+} is below $10^{11}m^{-3}$. These are used as the boundary conditions for impurity transport simulation inside the LCFS with IMPACT. It should be noted that the impurity density profile is strongly affected by the bulk plasma pedestal profiles primarily through mechanisms such as temperature screening effect. To access the sensitivity of impurity transport to pedestal structure, we examined the impact of varying the pedestal width Δ_{ped} using two values of C_{ped} : 0.076 and 0.089. It is worth noting that the former value has been shown to reproduce experimental data observed in JET-ILW pedestals at low gas fuelling rates [31], while the latter was proposed in [32] based on the ballooning critical pedestal model and has been validated with experimental data from DIII-D. Figures 3 (a) and (b) presents the pedestal profiles predicted by EPED1, based on the conditions determined using SONIC and Saarelma-Connor model. For the bulk plasma profiles, the pedestal height increases slightly with a wider Δ_{ped} , although the maximum value of pedestal current density $j_{\parallel,ped}$ remains nearly unchanged across the cases. As a result, $(T_{e,ped}, T_{i,ped})$ in keV is (1.04, 1.08) for

 $C_{ped} = 0.076$, and (1.19, 1.23) for $C_{ped} = 0.089$, respectively. In fact, as shown in the pedestal MHD stability diagram in the (j_{ped}, α) plane in Fig. 3 (c), the operation points are located near the "corner" of the diagram, suggesting that the plasma achieves optimal confinement performance, albeit with the presence of large type-I ELMs.

As a result of the difference in pedestal structure, the impurity density profiles and the corresponding Z_{eff} profiles vary, as shown in Fig. 4 (a). Since impurity transport in the pedestal region is governed by neoclassical mechanisms, and C_{6+} is the dominant impurity species inside the LCFS, the diffusivity D_{C6+} and the convective velocity v_{C6+} for each Δ_{ped} case are compared in Fig. 4 (b). In this comparison, all components contributing to the convective screening effect, $v_{C6+} > 0$, $v'_{C5+} > 0$, $n_{C6+} > 0$, $n'_{C6+} > 0$, are found to enhance the screening. These values are larger in the case where $C_{ped} = 0.089$ than in the case where $C_{ped} = 0.076$, indicating a stronger screening effect at the wider pedestal. This result is consistent with the differences in the n_{C6+} and Z_{eff} profiles shown in Fig. 4 (a).

Lastly, core transport simulations were conducted using GOTRESS within the GOTRESS+ code suite. As noted in the previous section, the final stationary condition is achieved by confirming the convergence across the core, pedestal and SOL/divertor regions with unchanged D2 gas puff rate as $\Gamma_{D2} = 5.5 \times 10^{21} s^{-1}$. The results are summarized in Table 2.

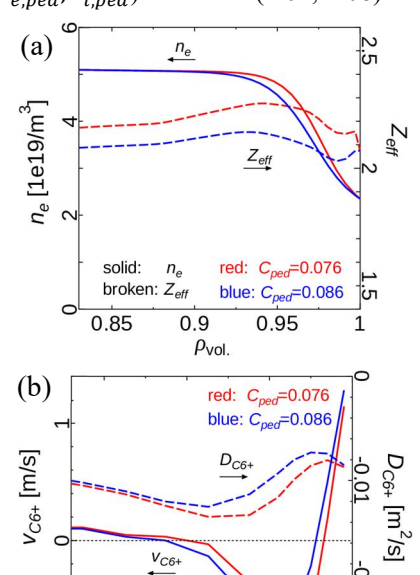


Figure 4: Profiles of (a) n_e and Z_{eff} , (b) v_{C6+} and D_{C6+} .

0.95

 V_{C6+} broken: D_{C6+}

0.9

solid:

0.85

C_{ped}	$q_{\parallel,max} = [MWm^{-2}]$	$n_{e,sep} = [10^{19} m^{-3}]$	$n_{e,ped} = [10^{19} m^{-3}]$	T _{e,ped} [keV]	T _{i,ped} [keV]	f_{GW}	β_N	H_{98y2}	$\langle Z_{eff} \rangle$	P _{sep} [MW]
0.076	9.69	2.35	5.05	1.04	1.08	0.74	2.68	1.10	2.10	15.41
0.089	9.71	2.35	5.05	1.19	1.23	0.74	2.78	1.14	2.01	15.45

TABLE 2. Summary of simulation results for JT-60SA baseline scenario

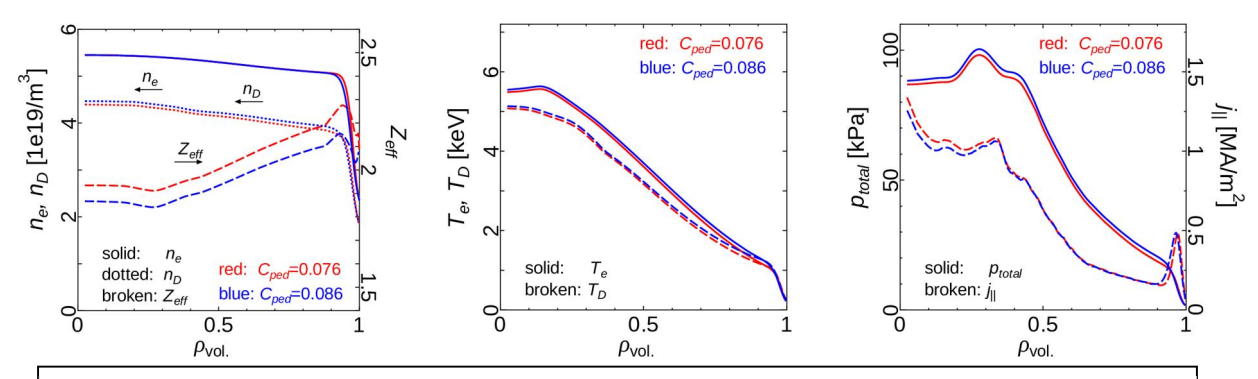


Figure 5: Plasma profiles of JT-60SA OP2 hybrid scenario plasma; (a) n_e , n_i and Z_{eff} , (b) T_e and T_i , (b) p and j_{\parallel} . Red (blue) line show them with $C_{ped} = 0.076$ (0.089) in EPED1.

In this case, the variation in C_{ped} has only a minor impact on Z_{eff} and the corresponding the power crossing the separatrix, P_{sep} . Consequently, the changes in $q_{\parallel,max}$ and $n_{e,sep}$ as determined by SONIC are confirmed to be negligibly small. Therefore, the differences in plasma performance parameters are primarily attributed to the variations in pedestal structure of the bulk plasma. Importantly, in both C_{ped} cases, the plasma performance parameters exceed the lower threshold values for the OP2 hybrid scenario, specifically $\beta_N > 2.0$ and $H_{98y2} > 1.1$, even under relatively high f_{GW} condition (~ 0.74). This represents the first result demonstrating that a JT-60SA stationary plasma, predicted by accounting for bulk plasma, impurity plasma and neutral behaviour across all regions inside the vacuum vessel, satisfies both the plasma performance criteria and engineering limit on divertor heat load.

3.3. Baseline scenario

Next, we predicted the JT-60SA baseline scenario using the same methodology as for the hybrid scenario. In this scenario, the heating power increases to $P_H = 26.5$ MW, and the plasma current rises to $I_p = 4.6$ MA. This implies that q_{\parallel} could exceed twice the value predicted in the hybrid scenario with $P_H = 19$ MW, $I_p = 2.7$ MA, where the estimation is based on the assumption $q_{\parallel} \propto P_{sep}B_t/\lambda_q B_p$, with $\lambda_q \propto I_p^{-1.19}$ following the Eich scaling, where B_t (B_p) is the toroidal (poloidal) magnetic field. Hence, a significant amount of D2 gas puff will be required to maintain $q_{\parallel} < 10$ MW m^{-2} . Therefore, we performed predictions for two cases; one in which only D2 gas is injected and another in which both D2 and Ne gases are injected to more effectively control q_{\parallel} .

Figure 6 presents the dependence of q_{\parallel} on Γ_{D2} in the two cases; note that in case with Ne seeding, $\Gamma_{Ne}=2.4\times10^{19}s^{-1}$ and $4.8\times10^{19}s^{-1}$ are tested. As shown in the figure, the required Γ_{D2} to achieve $q_{\parallel}\leq10MWm^{-2}$ decreases with increasing Ne injection. Specifically, the required fueling rates are $13.6\times10^{21}s^{-1}$ for the case without Ne, $11.0\times10^{21}s^{-1}$ for lower Ne seeding case, and $5.5\times10^{21}s^{-1}$ for higher Ne seeding case, respectively. These results clearly indicate that the required D2 gas puff rate is approximately 10 times larger than that used in the hybrid scenario, even when Ne puff is applied. Interestingly, $n_{e,sep}$ is not significantly affected by the Ne injection. The values obtained are $n_{e,sep}=(3.87,\ 3.40,\ 3.03)\times10^{19}m^{-3}$ for (w/o Ne, low Ne, high Ne) cases, respectively. It should be noted that the sensitivity of $n_{e,sep}$ to Γ_{D2} becomes weak when

 $\Gamma_{D2} \geq 5.0 \times 10^{21} s^{-1}$, suggesting that the neutral pressure in sub divertor region, $p_{0,div}$, becomes sufficiently high to saturate the response of $n_{e,sep}$ [33]. This trend is expected to be validated through future experiments in JT-60SA.

Using the specified fueling conditions for Γ_{D2} and Γ_{Ne} , we performed iterative simulation incorporating the physics of the core, pedestal and SOL/divertor regions. In these simulations, $C_{ped} = 0.089$ was assumed in EPED1. Table 3 summarizes the simulation results for each case. As shown, the target plasma parameters ($\beta_N \geq 2.0, H_{98y2} \geq 1.0$) are satisfied in the cases without Ne puff and with low Ne puff. In the case with high Ne puff, β_N is slightly reduced to 1.91; however, H_{98y2} remains above unity. Figure 7 compares the plasma profiles between the no-Ne and high-Ne puff cases. As illustrated, the degradation in β_N and H_{98y2} due to Ne puff is

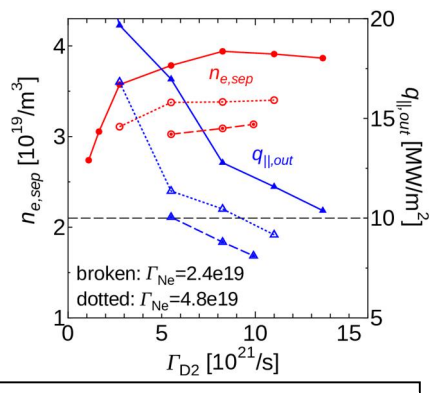


Figure 6: (a) Dependence of q_{\parallel} and $n_{e,sep}$ on Γ_{D2} .

mainly attributed to two factors: contamination of bulk ion plasma with Ne, and a reduction in pedestal pressure. The latter arises because the pedestal height is constrained by the amount of pedestal current as in the hybrid scenario case. An increase of pedestal density leads to higher collisionality, which in turn reduces the bootstrap current, thereby achieving higher pedestal height.

These results indicate that the JT-60SA baseline scenario is achievable as a standard H-mode scenario relevant to the ITER baseline, with performance targets of $\beta_N \geq 2.0$ and $H_{98y2} \geq 1.0$, even under stringent divertor heat load conditions. The pedestal density used in the simulations is predicted by a model validated against experiments, ensuring realistic boundary conditions. Notably, the required performance is maintained even when Ne is injected as an extrinsic radiative impurity to mitigate q_{\parallel} , demonstrating the robustness and flexibility of the scenario. These findings highlight the wide operational space available during the initial research phase of JT-60SA and support its role in preparation for ITER and future fusion reactors.

4. SUMMARY

This study presents GOTRESS+, a comprehensive physics-based simulation framework extended to predict stationary H-mode scenarios in JT-60SA's initial research phase. The framework integrates advanced codes—GOTRESS (core transport), ACCOME (magnetic equilibrium), OFMC (heating and fueling), EPED1 and Saarelma—Connor (pedestal structure), IMPACT (impurity transport), and SONIC (SOL/divertor)—to self-consistently evaluate plasma behavior across all regions.

The main objective is to demonstrate the feasibility of achieving high-performance, stationary plasmas in JT-60SA while satisfying engineering constraints on power exhaust. We focus on two representative Operational Phase 2 (OP2) scenarios: hybrid and baseline. Both are designed to meet ITER/DEMO-relevant goals, including high confinement ($H_{98y2} \ge 1.0$), elevated normalized beta ($\beta_N \ge 2.0$), and divertor heat flux (q_{\parallel}) below the engineering limit of $10MW/m^2$.

For the hybrid scenario, simulations show that stationary plasma conditions can be achieved without extrinsic impurity injection. Optimizing the deuterium fueling rate effectively mitigates divertor heat loads, while the predicted pedestal structure supports strong impurity screening. Plasma performance exceeds target thresholds, with $\beta_N \simeq 2.7$ and $H_{98y2} > 1.1$. The study also highlights the sensitivity of impurity transport and core plasma quality to pedestal width—wider pedestals enhance screening and reduce effective charge (Z_{eff}) .

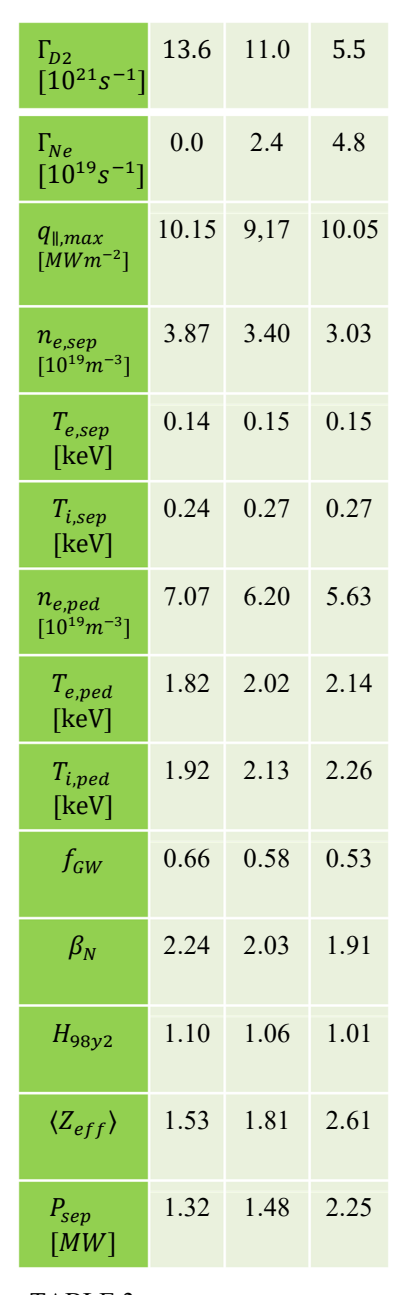


TABLE 3. Summary of simulation results for JT-60SA baseline scenario

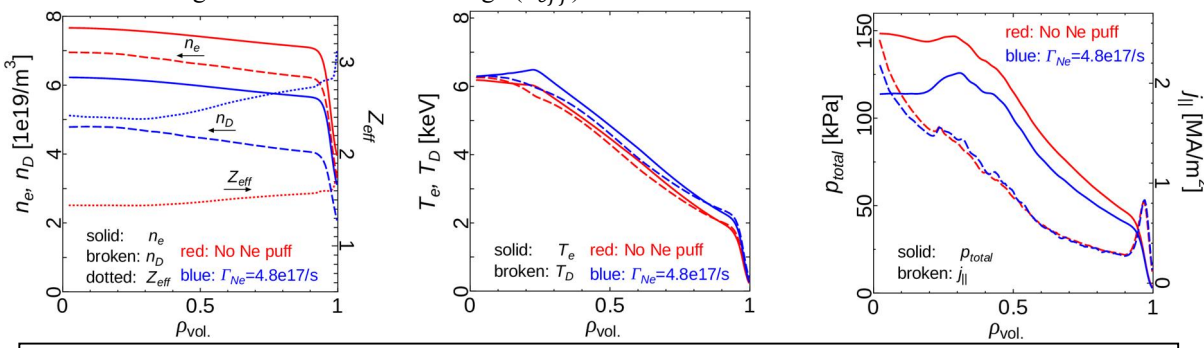


Figure 7: Plasma profiles of JT-60SA OP2 baseline scenario plasma; (a) n_e , n_i and Z_{eff} , (b) T_e and T_i , (b) p and j_{\parallel} . Red (blue) line show them with no Ne (with high Ne puff).

In the baseline scenario, with higher heating power and plasma current, the required deuterium fueling rate to control q_{\parallel} increases significantly. Simulations with and without neon (Ne) seeding show that Ne injection reduces the required D₂ fueling while maintaining acceptable heat loads. Even under high Ne puff, plasma performance remains viable, with β_N slightly reduced and H_{98y2} still above unity. Ne seeding causes modest degradation in pedestal pressure and core confinement due to increased collisionality and impurity content. The impact of Ne puff will be revisited with more sophisticated transport models, as those applied in the JET case [34].

These findings confirm JT-60SA's capability to support a wide operational space for stationary H-mode plasmas that meet both physics and engineering requirements. The integrated simulation approach offers a robust predictive tool for scenario planning and optimization, providing valuable insights for JT-60SA experiments and future reactor design.

ACKNOWLEDGEMENTS

The author (NA) gratefully acknowledges the insightful comments on our work from Drs. T. Suzuki and H. Urano.

REFERENCES

- [1] G. M. Staebler et al., Phys. Plasmas 12, 102508 (2005).
- [2] C. Bourdelle et al., Plasma Phys. Control. Fusion 58, 014036 (2016), J. Citrin et al., Plasma Phys. Control Fusion 59, 124005 (2017).
- [3] X. Bonnin et al, Plasma Fusion Rec. 11, 1403102 (2016), S. Wiesen et al., J. Nucl. Mater 463, 480 (2015).
- [4] H. Kawashima et al., Plasma Fusion Rec. 1, 031 (2006), K. Shimizu et al., Nucl. Fusion 49, 065028 (2009).
- [5] N. Asakura et al., Nucl. Fusion 61, 126057 (2021).
- [6] F. Maviglia et al., Nucl. Mater. Energy 26, 100897 (2021).
- [7] JT-60SA Research Unit « JT-60SA research plan (version 4.0), (2018).
- [8] M. Romanelli et al., Plasma Fusion Res. 9, 3403023 (2014).
- [9] N. Hayashi et al., Phys. Plasmas 17, 056112 (2010).
- [10] L. Garzotti et al., Nucl. Fusion 58, 026029 (2018).
- [11] S. Gabriellini et al., Nucl Fusion 65, 056041 (2025).
- [12] M. Honda et al., Nucl. Fusion 61, 116029 (2021).
- [13] S. Saarelma et al., Nucl. Fusion 63, 052002 (2023).
- [14] M. Honda, Comput. Phys. Commun 231, 94 (2018), M. Honda and E. Narita, Phys. Plasmas 26, 102307 (2019).
- [15] K. Tani et al., J. Comput. Phys. 98, 332 (1992).
- [16] K. Tani et al., J. Phys. Soc. Japan 50, 1726 (1981).
- [17] P. B. Snyder et al., Phys. Plasmas 16, 056118 (2009).
- [18] N. Hayashi et al., Nucl. Fusion 58, 066001 (2018).
- [19] W. A. Houlberg et al., Phys. Plasmas 4, 3230 (1997).
- [20] R. J. Groebner et al., Phys. Plasmas 9, 2134 (2002). M. A. Mahdavi et al., Phys. Plasmas 10, 3984 (2003).
- [21] S. Yamoto et al., Plasma Phys. Control. Fusion 62, 045006 (2020).
- [22] Y. R. Martin et al., J. Phys. : Conf. Ser. 123, 012033 (2008).
- [23] M. Erba et al., Plasma Phys. Control. Fusion 39, 261 (1997).
- [24] J. Garcia et al., Nucl. Fusion 2014,
- [25] N. Hayashi et al., Nucl. Fusion 2017
- [26] A. Redl et al., Phys. Plasmas 28, 022502 (2021).
- [27] R. Hulse, Nucl. Tech. Fusion 3, 259 (1983).
- [28] K. Hoshino et al., J. Nucl. Mater. 463, 573 (2015).
- [29] A. S. Kukushkin et al., J. Nucl. Mater. 337-9, 50 (2005).
- [30] T. Eich et al., Nucl. Fusion 53, 093031 (2013).
- [31] C. F. Maggi et al., Nucl. Fusion 55, 113031 (2015).
- [32] P. B. Snyder et al., Nucl Fusion 51, 103016, (2011)
- [33] D. Silvagni et al., Nucl. Mater. Energy 42, 101867 (2025).
- [34] S. Gabriellini et al., Nucl. Fusion 63, 086025 (2023).